Showcasing research from Professor Urakawa's laboratory, Department of Chemical Engineering, Delft University of Technology, Delft, The Netherlands.

From CO or CO_2?: space-resolved insights into high-pressure CO_2 hydrogenation to methanol over $Cu/ZnO/Al_2O_3$

With *operando* analytical methods based on Raman spectroscopy, gas chromatography and infrared thermography, gradients of reactants/products concentrations and temperature present in the catalytic reactor during high-pressure CO_2 hydrogenation to methanol were elucidated. The insights reveal temperature-dependent reaction pathways: direct CO_2-to-methanol is active at lower temperature, whereas CO-to-methanol pathway through reverse water-gas shift reaction is dominant at higher temperature over $Cu/ZnO/Al_2O_3$ catalyst.

As featured in:

ROYAL SOCIETY OF CHEMISTRY

rsc.li/catalysis

COMMUNICATION

Check for updates

From CO or CO$_2$?: space-resolved insights into high-pressure CO$_2$ hydrogenation to methanol over Cu/ZnO/Al$_2$O$_3$†

Rohit Gaikwad,‡[a] Helena Reymond,‡[b] Nat Phongprueksathat,‡[ac] Philipp Rudolf von Rohr[b] and Atsushi Urakawa (iD) *[acd]

The reaction pathway of high-pressure CO$_2$ hydrogenation over a Cu/ZnO/Al$_2$O$_3$ catalyst is investigated through the gradients of re-actants/products concentration and catalyst temperature within the catalytic reactor. This study reveals that methanol is formed through direct CO$_2$ hydrogenation at low temperature, while above 260 °C methanol formation is mediated via CO which is formed by reverse water–gas shift reaction.

The increasing atmospheric CO$_2$ concentration demands urgent actions to reduce CO$_2$ emission by converting CO$_2$ into useful chemicals and fuels. Among various chemicals derived from CO$_2$, methanol has considerable potential as a liquid fuel, hydrogen carrier, and C$_1$ feedstock.[1,2] Methanol can now be synthesized on commercially relevant scales via CO$_2$ hydrogenation over Cu/ZnO/Al$_2$O$_3$-based catalysts at 200–300 °C and 10–100 bar,[3,4] which is by far the most mature technology for efficient CO$_2$ conversion.[1] From a mechanistic point of view, methanol synthesis from CO$_2$ over Cu/ZnO/Al$_2$O$_3$ catalysts may occur through direct CO$_2$ hydrogenation (eqn (1)) or through reverse water–gas shift (RWGS) (eqn (2)) followed by CO hydrogenation (eqn (3)).[2]

$$CO_2 + 3H_2 \rightleftharpoons CH_3OH + H_2O \quad \Delta H_{298K, 5MPa} = -40.9 \text{ kJ mol}^{-1} \text{ (1)}$$

$$CO_2 + H_2 \rightleftharpoons CO + H_2O \quad \Delta H_{298K, 5MPa} = +49.8 \text{ kJ mol}^{-1} \quad (2)$$

$$CO + 2H_2 \rightleftharpoons CH_3OH \quad \Delta H_{298K, 5Mpa} = -90.7 \text{ kJ mol}^{-1} \quad (3)$$

[a] *Institute of Chemical Research of Catalonia (ICIQ), Av. Països Catalans 16, 43007 Tarragona, Spain*

[b] *Department of Mechanical Engineering, Institute of Process Engineering, ETH Zurich, Sonneggstrasse 3, 8092 Zürich, Switzerland*

[c] *Catalysis Engineering, Department of Chemical Engineering, Delft University of Technology, Van der Maasweg 9, 2629 HZ Delft, Netherlands. E-mail: A.Urakawa@tudelft.nl*

[d] *Japan Science and Technology Agency (JST), Gobancho, Chiyodaku, 102-0076 Tokyo, Japan*

† Electronic supplementary information (ESI) available. See DOI: 10.1039/d0cy00050g

‡ The three first authors contributed equally to this work.

Since methanol synthesis from CO$_2$ accompanies CO formation, the early studies concluded that CO hydrogenation is the main reaction pathway over Cu/ZnO catalysts.[5–7] However, the C^{18}O$_2$ isotopic labeling indicated that methanol can be produced from both CO and CO$_2$, by which CO$_2$ hydrogenation is the primary pathway at 220 °C.[8] The ^{14}CO and ^{14}CO$_2$ isotopic labeling also supported that CO$_2$ is the primary source of methanol instead of CO at 250 °C.[9] The intrinsic CO$_2$ hydrogenation rate is ~20 times faster than CO hydrogenation, especially at low conversion,[10] although the CO$_2$ hydrogenation is suppressed at high conversion due to water formation.[11] In contrast, DFT calculations showed the rate of the RWGS to form CO becomes ~100 times higher than CO$_2$ hydrogenation to methanol at a higher temperature (300 °C), in agreement with experiment.[12] However, such CO rather accumulates as a product since CO hydrogenation is slower than CO$_2$ hydrogenation. Another set of DFT calculations fitted to published experimental rate data under realistic conditions suggested that CO$_2$ hydrogenation is responsible for ~2/3 of methanol production.[13] It was later confirmed by isotope tracing experiments in ^{13}CO/^{12}CO$_2$/H$_2$ that CO$_2$ is the dominant carbon source in methanol product at 240 °C. However, the source of carbon gradually shifts from CO$_2$ to CO as the temperature is lowered (toward 160 °C).[14] It was proposed that CO hydrogenation could also be inhibited by the formation of formate intermediates at higher CO$_2$ concentrations (230 °C).[15,16] The isotopic labeling using H/D substitution suggested that methanol formation from CO$_2$ does not occur via consecutive RWGS and CO hydrogenation (at 250 °C),[17] and rather RWGS and CO$_2$ hydrogenation occur independently (220–260 °C).[17,18] Although some debates exist, methanol formation from CO$_2$ as the carbon source is currently the most widely accepted mechanism for Cu/ZnO-based catalysts, supported by both experimental findings and theoretical calculations mentioned above.

Thermodynamically, both CO and CO$_2$ hydrogenation reactions produce methanol, but the predominant reactions depend on the operating conditions.[19] The favorable conditions

for CO_2 hydrogenation to methanol are high pressure and low temperature according to Le Châtelier's principle, as obvious from eqn (1),[2] and the advantages of high-pressure reaction conditions above 200 bar in terms of CO_2 conversion (>90%), methanol selectivity (>95%) and methanol yield have been recently demonstrated.[20,21] In practice, however, there is an optimum reaction temperature where reaction kinetics are favorable, and simultaneously, endothermic RWGS does not rule the product selectivity. For example, in the previous studies (200 and 360 bar), the CO selectivity is surprisingly high at 170–200 °C, while it starts to decrease to the minimum as the temperature increases to 260 °C, indicating the CO hydrogenation towards the formation of methanol.[21] Similarly, CO selectivity increases at high space velocities, implying that CO-mediated path may be active under high-pressure conditions, which is indeed in accordance with early study at high pressure (415 bar).[5] Most mechanistic studies aiming at elucidation of the reaction pathway are performed at low to moderate pressure (<30 bar) and there are no convincing mechanistic clues reported to date for high-pressure methanol synthesis above such pressure.

This study aims at clarifying dominating reaction pathways and the source of carbon, CO or CO_2, resulting in methanol from the concentration profiles of the reactants/products as well as that of the catalyst temperature along the axial direction of the reactor packed with a commercial Cu/ZnO/Al_2O_3 catalyst at 200 and 360 bar (reactant pressure of 184 and 331 bar).[20,21] Changing space velocity by varying the reactant flow rate and/or catalyst amount is one way to gain the information;[22] however, this approach may influence mass transfer characteristics and also temperature gradient (higher mass flow rate can results in more prominent temperature gradient due to endo-/exo-thermicity of the reactions). In this study, we developed a method to study quantitatively the concentration of reactant/product fluids based on gas chromatography (GC) and Raman spectroscopy looking at different locations of the catalyst bed. Furthermore, infrared (IR) thermography was used to monitor the catalyst temperature under *operando* high-pressure reaction conditions to gain support on the reaction mechanisms through exo- and endo-thermicity.

The high-pressure reactor setup and used materials are explained in detail in ESI.† Briefly, the commercial Cu/ZnO/Al_2O_3 catalyst[20] was packed in a stainless steel (SS) or sapphire capillary reactor where three split catalyst beds were separated by empty spaces (P1–P4) for gas sampling and quantification. In the case of the SS reactor (Fig. 1A), the gas sampling for GC analysis was performed by needle valves connected to the void sections. The amount of the sampled gas was sufficiently small (confirmed by GC) so that it did not affect the overall catalytic activity. For Raman spectroscopic determination of fluid concentration, a Raman laser (532 nm) was focused onto the void sections filled with quartz wool in the sapphire reactor (Fig. 1B, S1 and S2,† holding reactant pressure up to 200 bar, 350 °C). The major advantage of the GC analysis is the accuracy in the quantifica-
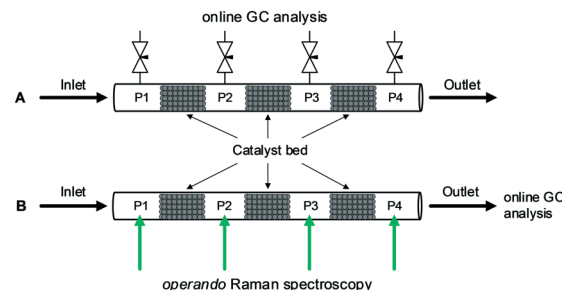

Fig. 1 Schematic of catalyst beds configuration for (A) a stainless-steel reactor with gas sampling valves at P1–P4, and (B) a sapphire reactor with Raman spectroscopic gas analysis at P1–P4 and gas chromatographic analysis at the outlet.

tion and that of the Raman analysis is the non-perturbing nature of the sampling on the flow behavior.

First, concentration profiling at P1–P4 was performed during CO_2 hydrogenation at the stoichiometric ratio (H_2/CO_2 = 3) in the SS reactor at three temperatures (180, 260 and 340 °C) and two pressure conditions (184 and 331 bar). CO_2 conversion and carbon-based mole fractions F (both in %), which are defined as CO_2 conversion scaled by respective product selectivity (that is in 0–1 scale, leading to $F_{CH_3OH} + F_{CO} = X_{CO_2}$). These quantities were used to understand in a facile fashion how much CO_2 is converted and into which product.
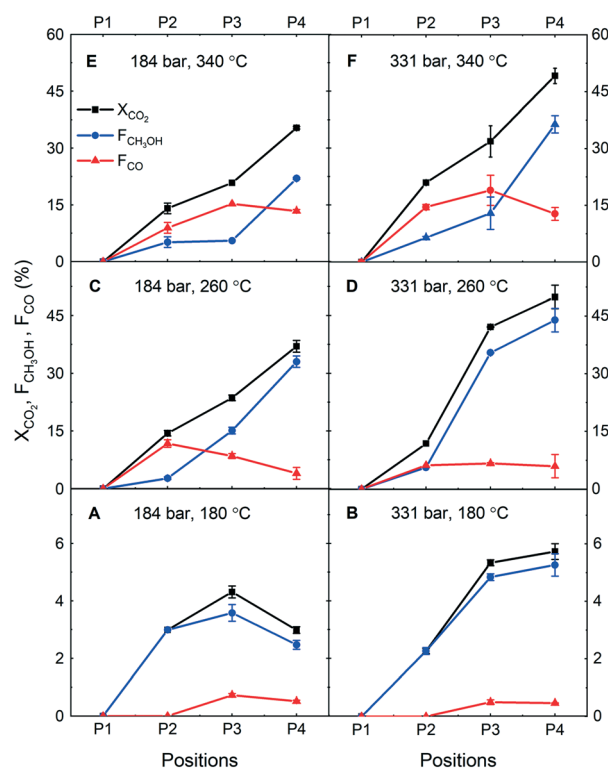

Fig. 2 CO_2 conversion (X_{CO_2}), the mole fraction of methanol (F_{CH_3OH}) and CO (F_{CO}) at different axial positions (P1–P4) during CO_2 hydrogenation to methanol over the commercial Cu/ZnO/Al_2O_3 catalyst. H_2/CO_2 = 3, T = 180, 260, and 340 °C, P = 184 and 331 bar, and GHSV = 10 000 h^{-1}.

2764 | *Catal. Sci. Technol.*, 2020, **10**, 2763–2768

This journal is © The Royal Society of Chemistry 2020

Fig. 2A and B show the catalytic performance in terms of X_{CO_2}, F_{CH_3OH} and F_{CO} at 180 °C at 184 bar and 331 bar, respectively. At this low reaction temperature, we observe low CO_2 conversion but high methanol selectivity, thus a high fraction of methanol. What is prominent are the X and F profiles and their differences. At this low conversion, virtually the partial pressure of the reactants (CO_2 and H_2) is unaltered throughout the catalyst bed and generally one expects little change in the reaction rate and product selectivity due to full kinetic control at different positions of the catalyst bed. However, this is not the case and lower CO_2 conversion is more prominent at the lower investigated pressure (184 bar, Fig. 2A) where CO_2 conversion does not linearly increase between $P2$–$P3$, and even drops between $P3$–$P4$. When the rate of CO_2 conversion is decreased, the fraction of methanol also decreases. Assuming that the intrinsic reaction selectivity at this temperature is almost 100% towards methanol (judging from the values at $P2$), the only explanation for the CO_2 conversion drop is methanol decomposition ($CH_3OH \rightarrow CO + 2H_2$),[23] especially between $P2$–$P3$. However, since the water partial pressure is expected to rise along with along the catalyst bed and the CO_2 conversion between $P3$–$P4$, steam reforming ($CH_3OH + H_2O \rightarrow CO_2 + 3H_2$) is supposed to take place. Although the reports on gas-phase methanol decomposition and steam reforming at such high pressure are expectedly limited, there is evidence suggesting that such reactions occur even at 250–450 bar under supercritical water,[24] and its kinetics can be enhanced as the number of collisions increases with pressure. Moreover, the slight decrease in CO fraction also indicates the forward water gas shift reaction. This explanation is also in accordance with high CO selectivity at low temperatures, as found in the previous work.[21] Based on the profiles of CO_2 conversion and product fractions, at 331 bar (Fig. 2B) this methanol decomposition and steam reforming to CO and CO_2 (generalized as "methanol decompositions") also takes place but to a significantly lesser extent. This is likely due to the pressure effects affecting to shift the equilibrium towards the product (methanol) side, showing one of the unique advantages of high-pressure reaction conditions.[20,21]

The same experiment was performed at two higher temperatures (260 and 340 °C) and the results obtained at 260 °C are summarized in Fig. 2C and D. First, the CO_2 conversion values are about one order of magnitude higher than those at 180 °C. Also, at both examined pressures, relatively high CO selectivity was observed. At 184 bar (Fig. 2C), CO was the major product, but then the fraction of CO decreased towards the outlet position. This is indicative of CO conversion to methanol, although there is a possibility of water–gas shift reaction forming CO_2 and H_2 from CO and H_2O (reverse reaction of eqn (2)). However, the methanol fraction drastically increases as CO fraction dropped towards the outlet direction. This indicates the former reaction (i.e. CO hydrogenation to methanol, eqn (3)) is likely the major active path under the studied reaction condition. At 331 bar (Fig. 2D) CO fraction remained relatively constant, whereas the methanol

fraction increased drastically along with CO_2 conversion between $P2$ and $P3$. At 184 bar (Fig. 2C) CO_2 conversion linearly increased and did not drop as observed at 180 °C. These results indicate three important insights into high-pressure CO_2 hydrogenation at 260 °C: (i) methanol formation is faster than its decompositions, (ii) CO_2 is constantly converted to methanol or CO as the intermediate at 184 bar and (iii) there is another factor promoting/enhancing CO_2 conversion at 331 bar. Regarding the point (ii), at 184 bar at $P2$, very high CO selectivity was observed and its continuous decrease and drastic increase in methanol production towards the reactor outlet implies that CO_2 is converted to CO at an almost constant rate and then CO is further converted to methanol. In this case, the latter reaction rate would mainly determine the final fraction of methanol and CO in the reactor. The point (iii) indicates the important effects of reaction pressure. According to Fig. S4 (ESI†), at 260 °C, we expect phase condensation at 331 bar but not at 184 bar. This may explain the sudden surge in CO_2 conversion between $P2$–$P3$; the CO_2 conversion was sufficiently high to reach the dew point of the condensable products (methanol and water) at this position in the reactor, positively impacting on the reaction rate or shifting the equilibrium towards methanol.

The presence of water in the fluid phase can promote Cu crystallite growth[25] and induce transformation of ZnO into $ZnCO_3$, as shown in the XRD patterns of spent catalysts (Fig. S3 and Table S1, ESI†). However, it is still difficult to establish the relationship between mechanism and catalyst structure from the existing results, especially using the bulk sensitive techniques.

Furthermore, the results obtained at the highest examined temperature (340 °C) are presented in Fig. 2E and F. Similar to the case of 260 °C, a large amount of CO was observed with a decrease in its fraction with respect to methanol towards the reactor outlet. On the other hand, CO_2 conversion increased almost linearly. These two observations indicate that RWGS is the first main step of CO_2 hydrogenation and produced CO reacts further with H_2 to produce methanol. It is also interesting to note the boosted methanol formation between $P3$–$P4$. A similar observation at 260 °C was interpreted to be caused by phase condensation. At this temperature, however, we do not expect such phase condensation to occur (Fig. S4, ESI†). One possibility may be a dense phase formation, like surface wetting, in the pore of the catalyst which is virtually identical to phase condensation. Besides, it is worth highlighting the maximum CO fraction observed in the reactor at 260 and 340 °C. According to the thermodynamic calculation (Fig. S5, ESI†), the equilibrium CO_2 conversions for RWGS at H_2/CO_2 = 3 are ca. 14% and 21% at 260 and 340 °C, respectively. A careful look in Fig. 2E and F shows that the CO fraction is close to the equilibrium CO_2 conversion in the middle of the reactor (since the fraction is the percentage of CO_2 converted to methanol; therefore, these numbers can be directly compared). Still, the CO fraction decreases accompanying the increase in methanol fraction close to the outlet of the reactor, implying that the

This journal is © The Royal Society of Chemistry 2020

Catal. Sci. Technol., 2020, 10, 2763–2768 | 2765

methanol synthesis rate is accelerated at the position. It is speculated that the dense phase formation over the catalyst accelerates CO hydrogenation to methanol. In addition, methanol decompositions may take place, but it is not possible to gain information about this point from the data obtained. Nevertheless, it is certain that the consumption rate of CO and CO_2 to form methanol is much greater than the methanol decompositions rate under these high-pressure conditions.

Based on the above studies, we conclude that the pressure effects on the reaction paths are relatively minor compared to the temperature effects, although increasing pressure is indeed advantageous for methanol synthesis because of favorable kinetics (more collisions), phase separation, and chemical equilibrium.[26] Interestingly, at 260 °C where we find optimum catalytic performance and liquid-phase condensation seems indeed to boost the reactivity of CO_2 to methanol by a concerted kinetic and thermodynamic interplay.

Furthermore, similar concentration profiling experiments were performed using Raman spectroscopy instead of GC. The major advantage of this spectroscopic approach is that the reaction and flow-patterns are not disturbed in contrast to the case of GC analyses. Fig. S6 (ESI†) shows a typical Raman spectrum of the reaction stream obtained at 260 °C at the outlet ($P4$). The rotational transitions of H_2 (355, 587, 812, 1033, 1246, 1447 cm^{-1}), as well as the Fermi dyad of CO_2 and satellite bands (1265, 1286, 1387, 1408 cm^{-1}), were clearly identified. Because of the small Raman scattering cross-section of CO, its characteristic feature at 2140 cm^{-1} was not sufficiently strong for quantitative analysis and only its formation could be confirmed at high CO concentration. The features at 2840 and 2945 cm^{-1} are attributed to methanol, showing a too weak signal for quantitative analysis. For these reasons, the intense bands of H_2 and CO_2 at 587 and 1387 cm^{-1}, respectively, were considered here to gain mechanistic insights.

Fig. 3 shows the evolution of the H_2/CO_2 ratio determined from the band areas at different void positions (Fig. 1) at 180 °C and 260 °C at 184 bar. The initial area ratio at $P1$ was scaled to 2.5 to represent the molar ratio of unreacted feed confirmed by GC measurements. The reaction at 180 °C

showed a slight decrease in the ratio moving from $P1$ to $P2$, before increasing towards $P3$, and no major change was observed moving from $P3$ to $P4$.

In the case of direct methanol synthesis from CO_2 (eqn (1)), 3 moles of H_2 would be consumed per mole of CO_2 for the production of methanol, rendering H_2 the limiting reactant in our experimental condition (feed H_2/CO_2 = 2.5). On the other hand, if CO_2 is consumed to form CO via RWGS (eqn (2)), CO_2 would become a limiting reactant. Therefore, a decrease in the H_2/CO_2 ratio would signify an excessive H_2 consumption as in the former case of direct methanol synthesis, whereas an increase in the ratio would be a sign of a gradual CO_2 shortage by RWGS. In case methanol is a secondary product obtained from the subsequent hydrogenation of CO, as a net, the ratio is expected to decrease as an equivalent amount of H_2 is required whichever the CO_x (x = 1 or 2) is the carbon source in the methanol. The initial slight decrease in the ratio at $P1$–$P2$ at 180 °C implies direct methanol synthesis reaction. Then at $P2$–$P3$, the ratio increases, which is indicative of RWGS. However, as discussed above, this is most likely due to the decompositions of methanol since such drastic selectivity change is unlikely at the low CO_2 conversion level. The increase in the ratio is therefore attributed to methanol decompositions, which is fully consistent with the observation and the previous results at 180 °C (Fig. 2). In this Raman study, however, the ratio did not increase further as expected from the results in Fig. 2. This may be due to the higher space velocity of this Raman study compared to the study by GC and consequent less pronounced change in the ratio from less prominent methanol decompositions.

At 260 °C there was a clear initial increase of the ratio and then decrease towards the outlet (Fig. 3). The increasing ratio indicates the increase in the amount of CO by RWGS in the reactor and then subsequent decrease indicates the increase in the amount of methanol, no matter which reaction paths (eqn (1) vs. eqn (3)) are active. This profile is in full accordance with the results presented in Fig. 2 obtained in a comparable reaction condition where initially CO was produced and then CO was hydrogenated to methanol.

The sharp drop in the ratio at 260 °C coincided with the observation of condensation as liquid droplets at the rear end of the packed bed at $P4$ (Fig. S8, ESI†). As discussed above, the condensation is attributed to enhanced methanol synthesis via CO or CO_2, by in situ separation of the less volatile components, namely water and methanol. Indeed, upon focusing the Raman laser spot on the condensed phase, more intense methanol peak was observed, and the H_2/CO_2 ratio dropped to further lower values, suggesting the higher miscibility of CO_2 than H_2 in the condensed phase. According to the thermodynamic expectations at $CO_2 : H_2$ = 1:3 (Fig. S4, ESI†), liquid phase condensation is not expected at 184 bar, 260 °C.

Lastly, IR thermography was used to measure the temperature of the catalyst bed under the reaction in order to validate the sequential nature of the methanol formation (RWGS and CO hydrogenation to methanol) from the endo-/exo-
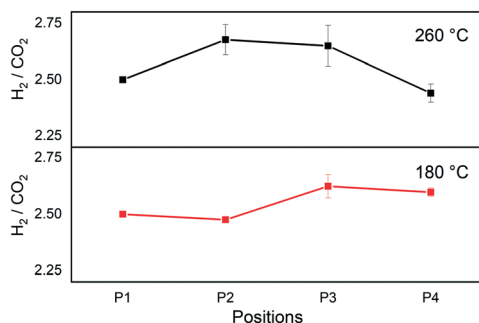

Fig. 3 H_2/CO_2 ratio at different positions during CO_2 hydrogenation to methanol over the commercial $Cu/ZnO/Al_2O_3$ catalyst. H_2/CO_2 = 2.5, T = 180 and 260 °C, P = 184 bar, and GHSV = 80 000 h^{-1}.

2766 | Catal. Sci. Technol., 2020, **10**, 2763–2768
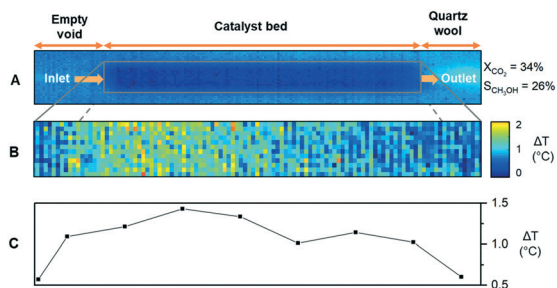
This journal is © The Royal Society of Chemistry 2020

Fig. 4 (A) IR thermogram of catalyst bed at room temperature, (B) subtracted IR thermogram at reaction temperature, and (C) temperature deviation (ΔT) profile along the catalyst bed during CO_2 hydrogenation to methanol over the commercial $Cu/ZnO/Al_2O_3$ catalyst. $H_2/CO_2 = 3$, $T = 340$ °C, $P = 184$ bar, and GHSV = 80 000 h^{-1}.

thermicity of the reactions (eqn (1)–(3)). The reaction was performed at the stoichiometric ratio at 184 bar in a sapphire reactor similar to the Raman study without separating the catalyst bed, as shown in Fig. 4A. At 180 °C, the IR signal, as well as CO_2 conversion, were too low to detect changes in the temperature of the catalyst bed. Thus, the experiments were performed at 260 and 340 °C. To detect subtle differences in the temperature of the catalyst bed, the thermogram showing a temperature distribution is obtained by the subtraction of thermograms during reaction and calibration, as shown in Fig. S9 (ESI†).

The differential IR thermogram (Fig. 4B) displays an exo-thermic region of the catalyst bed during the reaction. The differential temperature profiles (Fig. 4C) are calculated from the radial temperature average along the catalyst bed. Evidently, the temperature profile at 340 °C is spatially varying. A relatively colder region located close to the front of the catalyst bed at 340 °C and subsequent temperature increase (then decrease) along the flow direction indicate endothermicity of RWGS near the fluid inlet and then methanol is formed. Such a temperature variation along the catalyst bed is barely observable at 260 °C (Fig. S10†), indicating that RWGS and CO hydrogenation likely occur in close proximity and cause overlapping of the two regions. The results at two different temperatures are in line with the methanol and CO selectivity profiles and the reaction mechanisms suggested above.
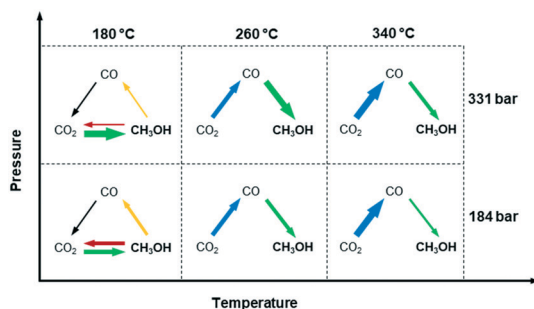

Fig. 5 Major reaction pathways in high-pressure CO_2 hydrogenation over $Cu/ZnO/Al_2O_3$ catalyst at 180 °C, 260 °C and 340 °C at 184 and 331 bar. The width of the arrow shows the amount of one species transformation to others.

In conclusion, the effects of temperature and pressure on reaction pathways were clarified by the space-resolved methodologies under *operando* conditions. Temperature has a significant influence on the dominant reaction pathways of methanol synthesis, as summarized in Fig. 5. It is confirmed that methanol is produced *via* direct CO_2 hydrogenation at 180 °C, and *via* RWGS and CO hydrogenation at 260–340 °C. This could be explained by the limited RWGS activity at 180 °C, and more dominant RWGS activity as temperature increases. Moreover, there is a sign that methanol could possibly decompose or be steam reformed after formation, which is effectively suppressed by increasing pressure. Although pressure seems to have no influence on the reaction pathways, it greatly enhances methanol selectivity by inducing *in situ* condensation. This work demonstrates how spatially resolved *operando* study can be performed at high-pressure conditions to gain insights into the reaction mechanisms that have practical implications of potential advantages of multicomponent catalysts (*i.e.* selective in CO or CO_2 to methanol) in a reactor.

Conflicts of interest

There are no conflicts to declare.

Acknowledgements

References

1 A. Goeppert, M. Czaun, J.-P. Jones, G. K. Surya Prakash and G. A. Olah, *Chem. Soc. Rev.*, 2014, **43**, 7995–8048.
2 A. Álvarez, A. Bansode, A. Urakawa, A. V. Bavykina, T. A. Wezendonk, M. Makkee, J. Gascon and F. Kapteijn, *Chem. Rev.*, 2017, **117**, 9804–9838.
3 G. A. Olah, *Angew. Chem., Int. Ed.*, 2013, **52**, 104–107.
4 G. A. Olah, A. Goeppert and G. K. S. Prakash, *Beyond Oil and Gas: The Methanol Economy*, Wiley, 2009, vol. 44.
5 V. N. Ipatieff and G. S. Monroe, *J. Am. Chem. Soc.*, 1945, **67**, 2168–2171.
6 K. Klier, *Adv. Catal.*, 1982, **31**, 243–313.
7 K. Klier, V. Chatikavanij, R. G. Herman and G. W. Simmons, *J. Catal.*, 1982, **74**, 343–360.
8 G. Liu, D. Willcox, M. Garland and H. H. Kung, *J. Catal.*, 1985, **96**, 251–260.
9 G. C. Chinchen, P. J. Denny, D. G. Parker, M. S. Spencer and D. A. Whan, *Appl. Catal.*, 1987, **30**, 333–338.
10 M. Sahibzada, I. S. Metcalfe and D. Chadwick, *J. Catal.*, 1998, **174**, 111–118.
11 C. V. Ovesen, B. S. Clausen, J. Schiøtz, P. Stoltze, H. Topsøe and J. K. Nørskov, *J. Catal.*, 1997, **168**, 133–142.

This journal is © The Royal Society of Chemistry 2020

Catal. Sci. Technol., 2020, **10**, 2763–2768 | **2767**

12 Y. Yang, J. Evans, J. A. Rodriguez, M. G. White and P. Liu, *Phys. Chem. Chem. Phys.*, 2010, **12**, 9909.

13 L. C. Grabow and M. Mavrikakis, *ACS Catal.*, 2011, **1**, 365–384.

14 Y. Yang, C. A. Mims, D. H. Mei, C. H. F. Peden and C. T. Campbell, *J. Catal.*, 2013, **298**, 10–17.

15 F. Studt, M. Behrens, E. L. Kunkes, N. Thomas, S. Zander, A. Tarasov, J. Schumann, E. Frei, J. B. Varley, F. Abild-Pedersen, J. K. Nørskov and R. Schlögl, *ChemCatChem*, 2015, **7**, 1105–1111.

16 W. J. Van Rensburg, M. A. Petersen, M. S. Datt, J. A. Van Den Berg and P. Van Helden, *Catal. Lett.*, 2015, **145**, 559–568.

17 E. L. Kunkes, F. Studt, F. Abild-Pedersen, R. Schlögl and M. Behrens, *J. Catal.*, 2015, **328**, 43–48.

18 A. Karelovic, G. Galdames, J. C. Medina, C. Yévenes, Y. Barra and R. Jiménez, *J. Catal.*, 2019, **369**, 415–426.

19 X.-M. Liu, G. Q. Lu, Z.-F. Yan and J. Beltramini, *Ind. Eng. Chem. Res.*, 2003, **42**, 6518–6530.

20 R. Gaikwad, A. Bansode and A. Urakawa, *J. Catal.*, 2016, **343**, 127–132.

21 A. Bansode and A. Urakawa, *J. Catal.*, 2014, **309**, 66–70.

22 S. K. Wilkinson, L. G. A. Van De Water, B. Miller, M. J. H. Simmons, E. H. Stitt and M. J. Watson, *J. Catal.*, 2016, **337**, 208–220.

23 Y. Choi and H. G. Stenger, *Appl. Catal., B*, 2002, **38**, 259–269.

24 N. Boukis, V. Diem, W. Habicht and E. Dinjus, *Ind. Eng. Chem. Res.*, 2003, **42**, 728–735.

25 J. T. Sun, I. S. Metcalfe and M. Sahibzada, *Ind. Eng. Chem. Res.*, 1999, **38**, 3868–3872.

26 J. G. van Bennekom, R. H. Venderbosch, J. G. M. Winkelman, E. Wilbers, D. Assink, K. P. J. Lemmens and H. J. Heeres, *Chem. Eng. Sci.*, 2013, **87**, 204–208.

2768 | *Catal. Sci. Technol.*, 2020, **10**, 2763–2768

This journal is © The Royal Society of Chemistry 2020